Supporting Information

Photo-activated autophagy-associated tumor cell death by lysosome impairment based on manganese-doped graphene quantum dots

Qingjng Liang,[#a] Feng Yu,[#a] Hao Cai,[b] Xiaoyan Wu,[b] Menghui Ma,[a] Zijian Li,*[b] Antonio Claudio Tedesco,[ac] Junfa Zhu,[d] Qian Xu,[d] Hong Bi*[b]

[a] *School of Chemistry and Chemical Engineering, Anhui University, Hefei 230601, China.*

[b] *School of Materials Science and Engineering, Anhui University, Hefei 230601, China.*

[c] *Department of Chemistry, Center of Nanotechnology and Tissue Engineering-Photobiology and Photomedicine Research Group, Faculty of Philosophy, Sciences and Letters of Ribeirão Preto, University of São Paulo, Ribeirão Preto, São Paulo 14040-901, Brazil. National Synchrotron Radiation Laboratory, University of Science and Technology of China, Hefei, Anhui 230029, China.*

[d] *National Synchrotron Radiation Laboratory, University of Science and Technology of China, Hefei, Anhui 230029, China.*

*E-mail: bihong@ahu.edu.cn; 22018@ahu.edu.cn

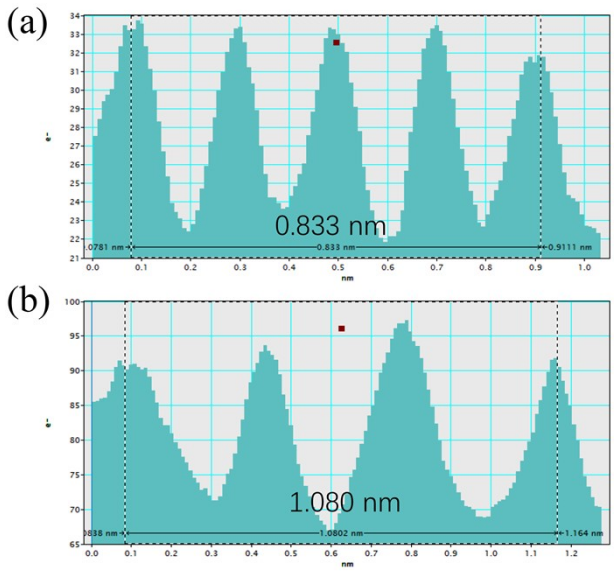

Figure S1. Line profile of diffraction fringes for the (a) FGQDs and (b) Mn-FGQDs.

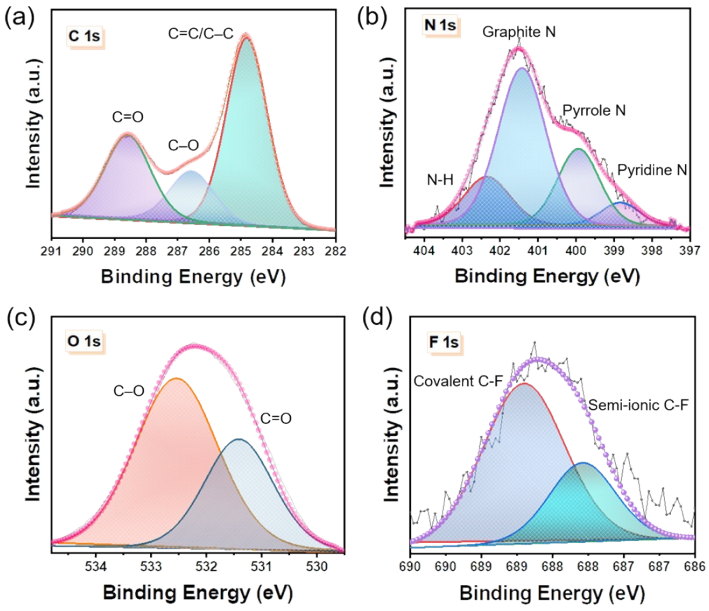

Figure S2. The high-resolution (a) C 1s, (b) N 1s, (c) O 1s and (d) F 1s spectra of FGQDs.

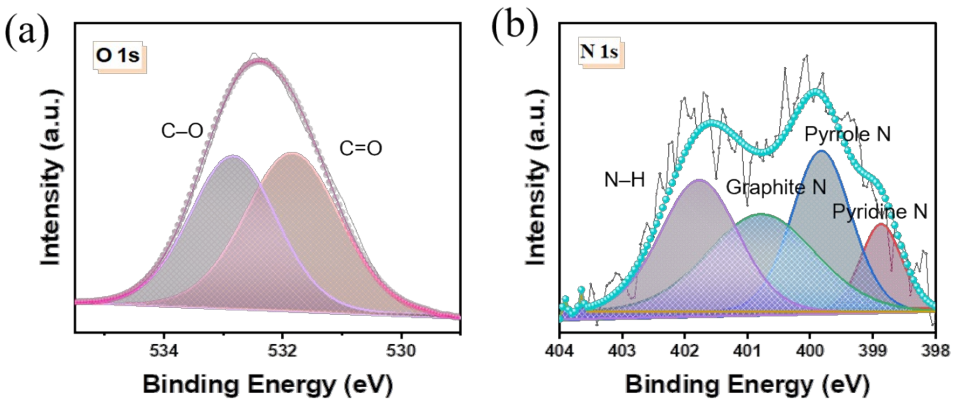

Figure S3. The high-resolution (a) O 1s and (b) N 1s spectra of Mn-FGQDs.

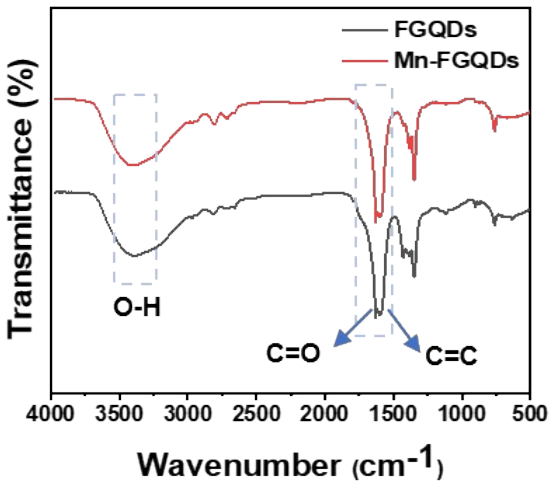

Figure S4. Fourier transform infrared spectra of FGQDs and Mn-FGQDs.

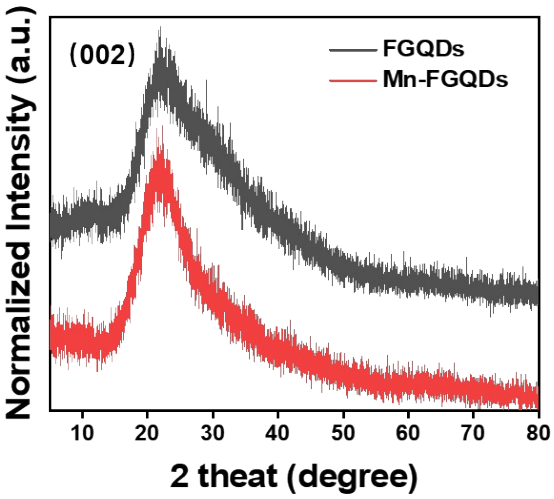

Figure S5. The XRD patterns of FGQDs and Mn-FGQDs powder.

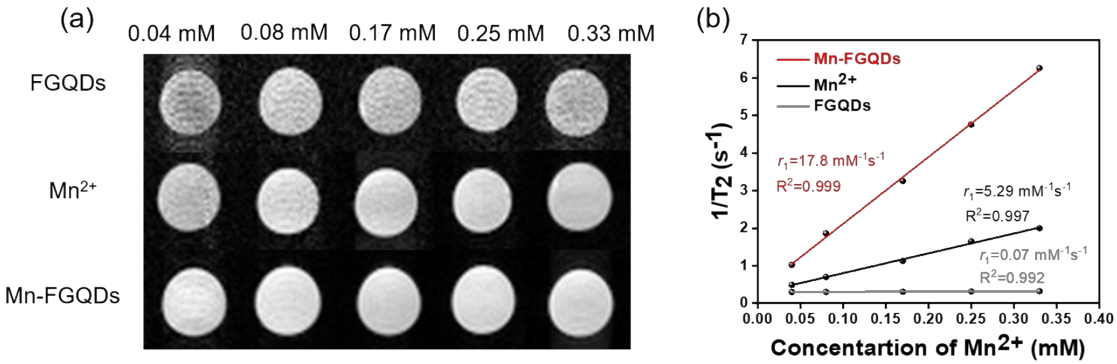

Figure S6. T_1-weighted MRI images (a) and r_1 relaxation rate images (b) of Mn-FGQDs, Mn^{2+}, and FGQDs.

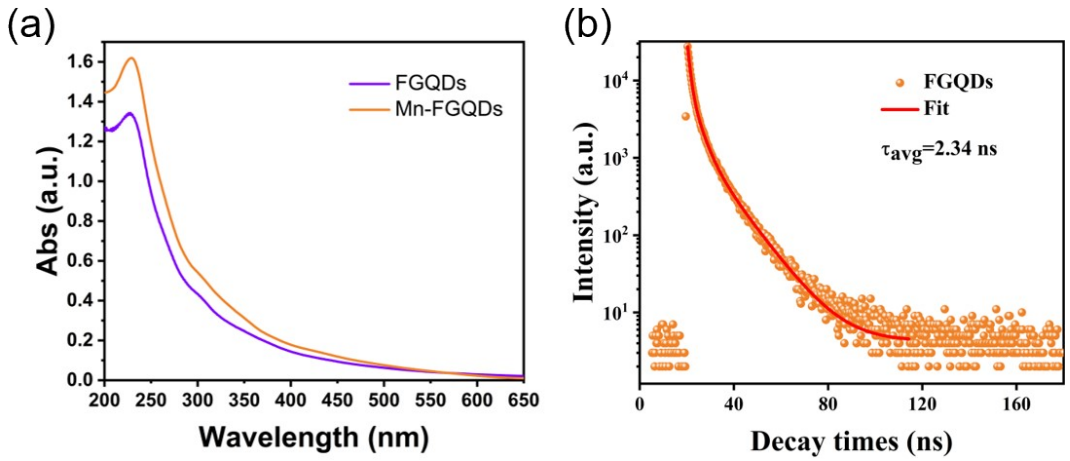

Figure S7. (a) UV-vis absorption spectra of the FGQD and Mn-FGQDs. (b) Fluorescence decay spectra of FGQDs.

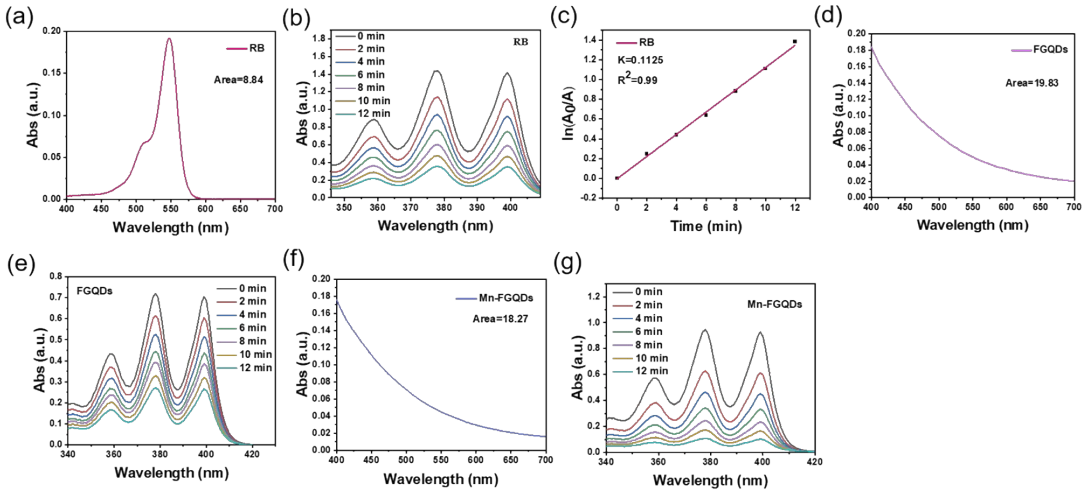

Figure S8. UV-vis absorption spectra of (a) RB, (d) FGQDs, and (f) Mn-FGQDs. The UV-vis absorption spectra of ABDA decomposed by (b) RB, (e) FGQDs, and (g) Mn-FGQDs at different LED lamp irradiation times. Decomposition rate constants of ABDA by (c) RB.

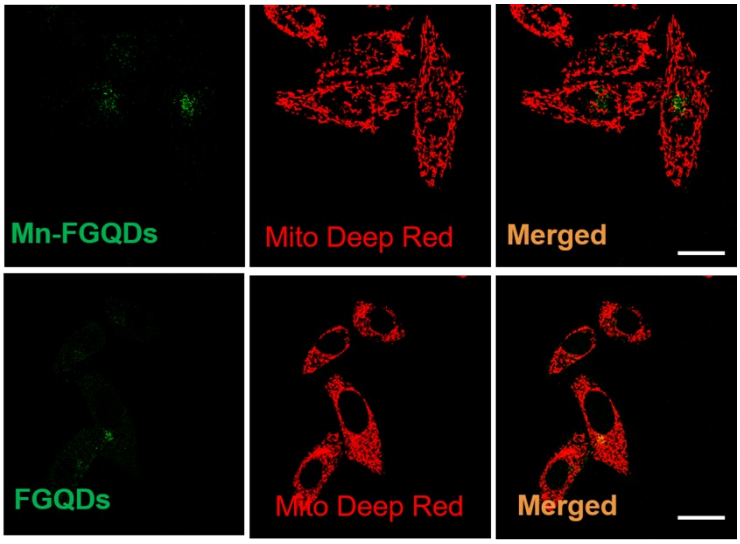

Figure S9. Confocal fluorescence images of HepG2 cells stained by Mito-Deep Red tracker after incubation with FGQDs and Mn-FGQDs (200 μg mL^{-1}) for 4 h, respectively. Scale bar = 30 μm.

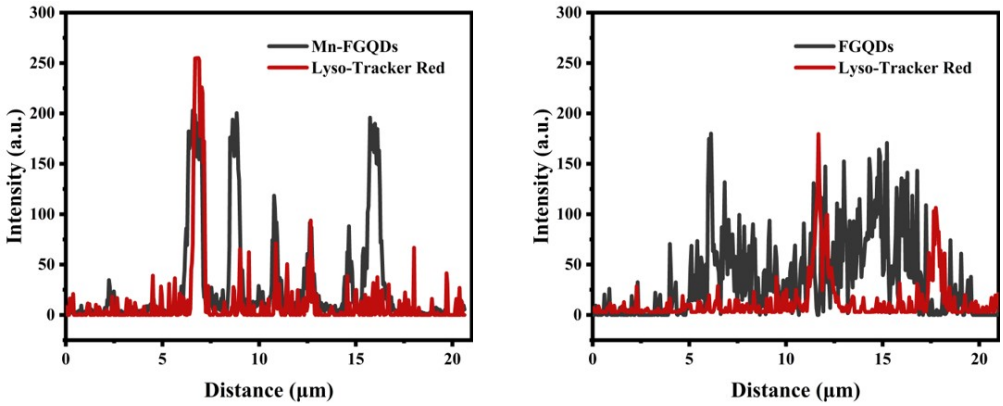

Figure S10. The fluorescence intensity curve between the green and red channels in HepG2 cells.

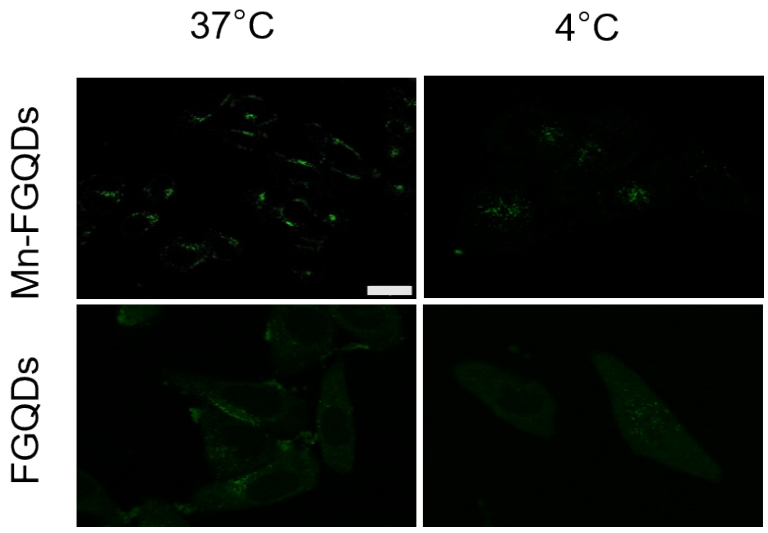

Figure S11. Confocal fluorescence images of HepG2 cells incubated at 37°C or 4°C and then treated with FGQDs or Mn-FGQDs for 4 h. Scale bar = 20 μm.

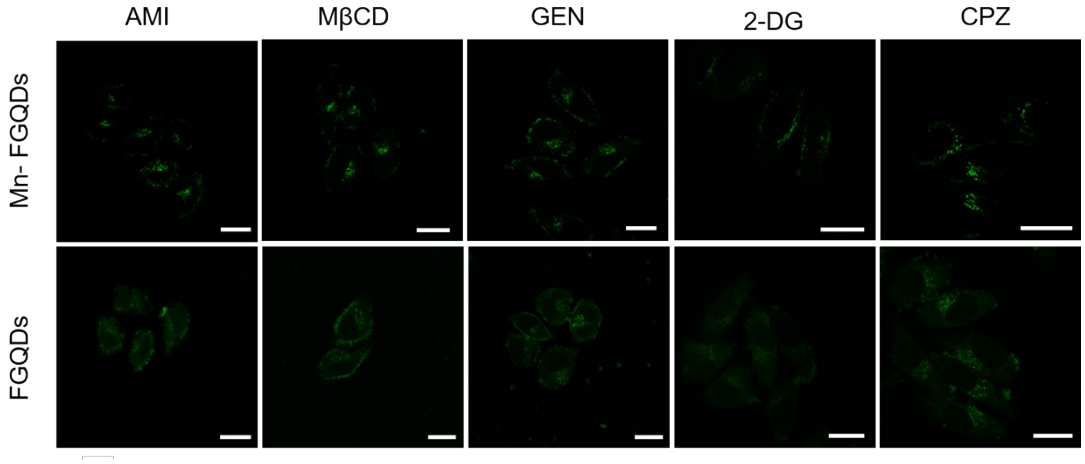

Figure S12. Fluorescence images of HepG2 cells incubated with the FGQDs and Mn-FGQDs in the presence of different endocytosis inhibitors such as AMI, MβCD, GEN, 2-DG, and CPZ. Scale bar = 20 μm.

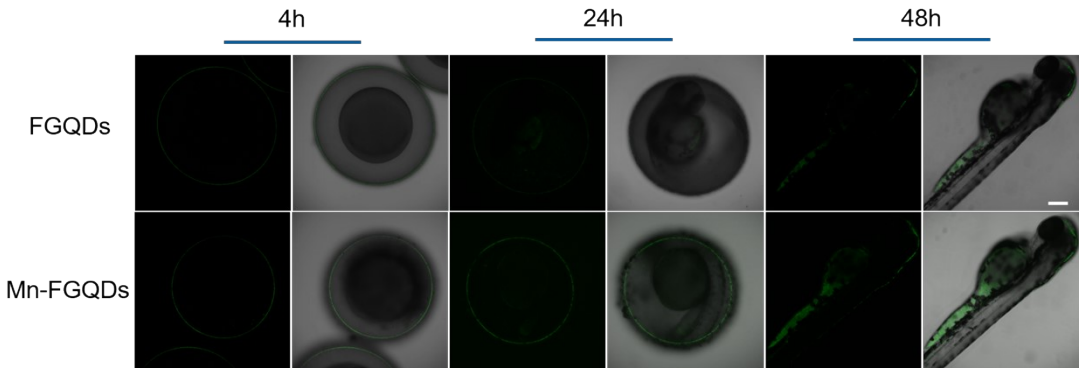

Figure S13. CLSM images of zebrafish embryos and juveniles at different incubation times. Scale bar = 200 μm.

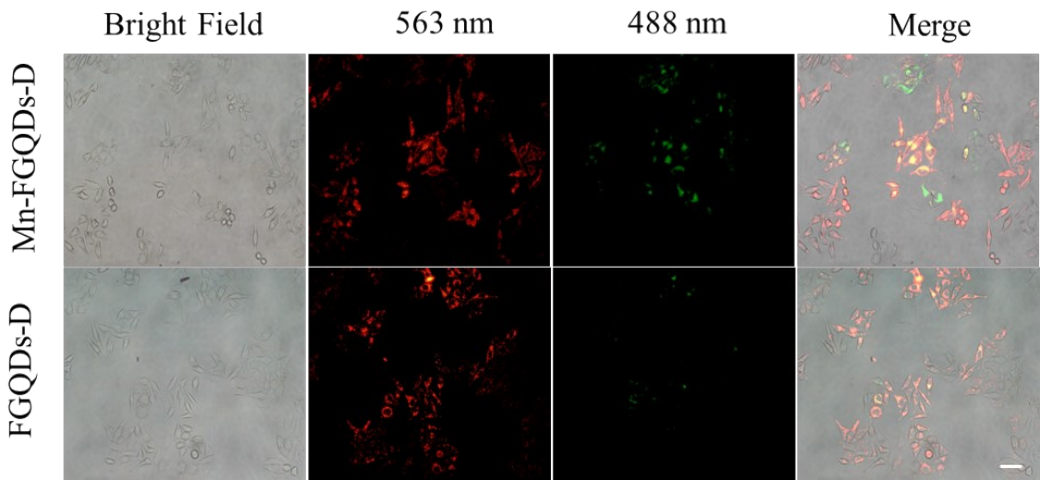

Figure S14. CLSM images of living HepG2 cells co-cultured with FGQDs and Mn-FGQDs labelled with JC-1 were taken before LED irradiation (400–500 nm and 65 mW cm^{-2}) for 12 min. Scale bar = 50 μm.

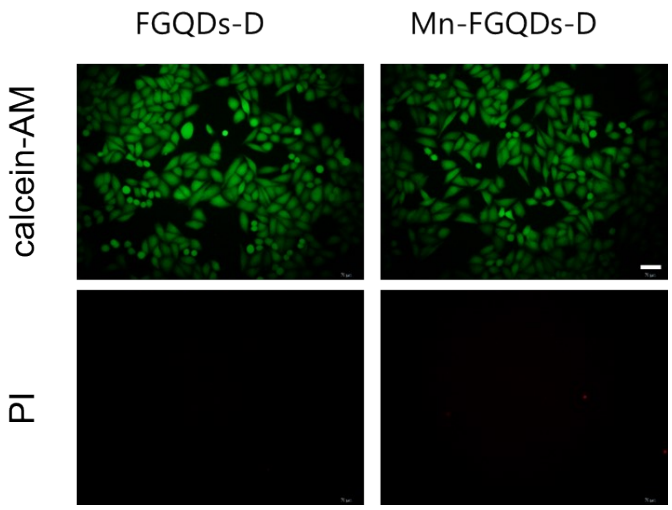

Figure S15. Fluorescence images of living HepG2 cells treated with FGQDs and Mn-FGQDs solutions for 4 h and labelled with calcein-AM and of dead cells labelled with PI before LED irradiation (400–500 nm and 65 mW cm^{-2}) for 12 min, respectively. Scale bar = 50 μm.

Table S1. The saturation magnetization (Ms) and magnetic coercivity (Hc) of FGQDs and Mn-FGQDs at 300 and 5 K.

T (K)	FGQDs		Mn-FGQDs	
	M_S (emu/g)	H_C (Oe)	M_S(emu/g)	H_C (kOe)
300	0.052	92.84	1.148	31.53
77	0.069	33.03	1.555	29.17